PROCEEDINGS OF SCIENCE

Performance of the ASTRI Mini-Array with different levels of night-sky background

F. G. Saturni,[a,b,*] **S. Lombardi,**[a,b] **L. A. Antonelli,**[a] **C. Bigongiari,**[a,b] **E. Fedorova,**[a] **A. Giuliani,**[c] **F. Lucarelli,**[a,b] **M. Mastropietro,**[a] **G. Pareschi**[d] **for the ASTRI Project**[e]

[a] *INAF – Osservatorio Astronomico di Roma, Via Frascati 33, I-00078 Monte Porzio Catone (RM), Italy*
[b] *ASI – Space Science Data Center, Via del Politecnico s.n.c., I-00133 Roma, Italy*
[c] *INAF – Istituto di Astrofisica Spaziale e Fisica Cosmica, Via A. Corti 12, I-20133 Milano, Italy*
[d] *INAF – Osservatorio Astronomico di Brera, Via E. Bianchi 46, I-23807 Merate (LC), Italy*
[e] *http://www.astri.inaf.it/en/library/*

E-mail: francesco.saturni@inaf.it, saverio.lombardi@inaf.it

The ASTRI Mini-Array is an array of nine small-sized (4-m diameter) and large field of view (∼10°) imaging atmospheric Cherenkov telescopes under deployment at the *Observatorio del Teide* (Tenerife, Spain). The system is sensitive to γ-ray radiation in the energy range $1 \div 200$ TeV. The telescopes are characterized by a dual-mirror optical system and equipped with silicon photo-multiplier cameras. These sensors can be operated under relatively high levels of night-sky background, thus allowing us to extend the duty cycle of Cherenkov observations beyond the "dark" regime alone. In order to assess the performance of the system with different night-sky brightness conditions, a study of the intensity and spectral shape of the illumination at the Teide Observatory site as a function of the array pointing direction and of the lunar phase has been carried out. Then, dedicated Monte Carlo simulations have been generated with a set of increasing brightness levels and subsequently reduced with `A-SciSoft` (ASTRI Scientific Software), the official scientific software package of the ASTRI Project. In this contribution, we present the performance of the ASTRI Mini-Array achieved with the aforementioned MC simulations, discussing the implications of our finding on the duty cycle of the system and its scientific potentialities.

The 38th International Cosmic Ray Conference (ICRC2023)
26 July – 3 August, 2023
Nagoya, Japan

*Speaker

PoS(ICRC2023)717

1. Introduction

The ASTRI Mini-Array [1, 2] is an INAF project aimed to observe astronomical sources emitting at very high-energy (VHE) in the multi-TeV spectral band, consisting of an array of nine innovative imaging air Cherenkov telescopes (IACTs; [3]) that are an evolution of the two-mirror ASTRI-*Horn* telescope successfully tested since 2014 at the INAF "M. C. Fracastoro" observing station in Serra La Nave (Mt. Etna, Italy) [4, 5]. The nine telescopes are being installed at the *Observatorio del Teide* in Tenerife (Canary Islands, Spain).

Both the assessment of the system performance and the analysis of real Cherenkov data rely on the production of suitable Monte Carlo (MC) simulations, taking advantage of a dedicated software chain [6]. In this framework, the evaluation of the ASTRI Mini-Array performance across the entire window of useful observing time for Cherenkov data-taking relies upon the determination of intensity and spectral shape of the night-sky background (NSB) as a function of the array pointing direction and the lunar phase; in particular, the latter parameter is of paramount importance to maximize the window of useful observing time, not limiting the instrument's duty cycle to the "dark" regime alone [7]. One of the major critical tasks to be tackled for this analysis is thus the production of adequate MC simulations satisfying the desired NSB requirements.

In this contribution, we describe the estimates of the NSB levels used in the MC simulations, under different operating conditions of the ASTRI Mini-Array. The main goals of this work are: (i) the determination of an average integrated level of NSB in Moonless (dark) nights at the Teide site that immediately yields the site "quality" [8]; (ii) the construction of a (coarse) 2D NSB sky distribution in dark conditions, in order to highlight over-luminous directions; (iii) the study of how the presence of the Moon alters NSB intensity depending on the Moon phase and pointing distance, to be accounted in simulations, duration estimates of the observing windows and scheduling procedures; and (iv) the comparison between the ASTRI Mini-Array performance with increasing NSB levels for several pointing zenith angles (ZAs), starting from standard low values (20°).

2. Determination of the Teide night-sky brightness with Moon

The information on the illumination level of the night sky at a given astronomical site can be obtained by computing the expected NSB spectrum from prime principles, using command-line and/or online tools such as e.g. SkyCalc provided by the European Southern Observatory (ESO)[1]. This tool is based on existing, well validated sky models [9, 10], and has already been extensively used for the determination of the NSB spectrum at several observing sites [11, 12].

In this way, we compute the NSB spectrum for all the combinations of five different Moon phases (from new to full) and Moon pointing distances (60°, 40°, and 20°). The dark NSB synthetic spectrum obtained in this way is shown in Fig. 1. We note that the synthetic NSB spectrum produced with SkyCalc is strictly valid for the La Silla ESO site, rather than for the Teide site; since a precise spectral measurement of the NSB spectrum at our site of interest is not presently available, a rescaling of the dark NSB synthetic spectrum to its actual brightness conditions must be performed in order to obtain a closer match with the expected sky illumination.

[1]Available at: http://www.eso.org/observing/etc/doc/skycalc/helpskycalc.html.

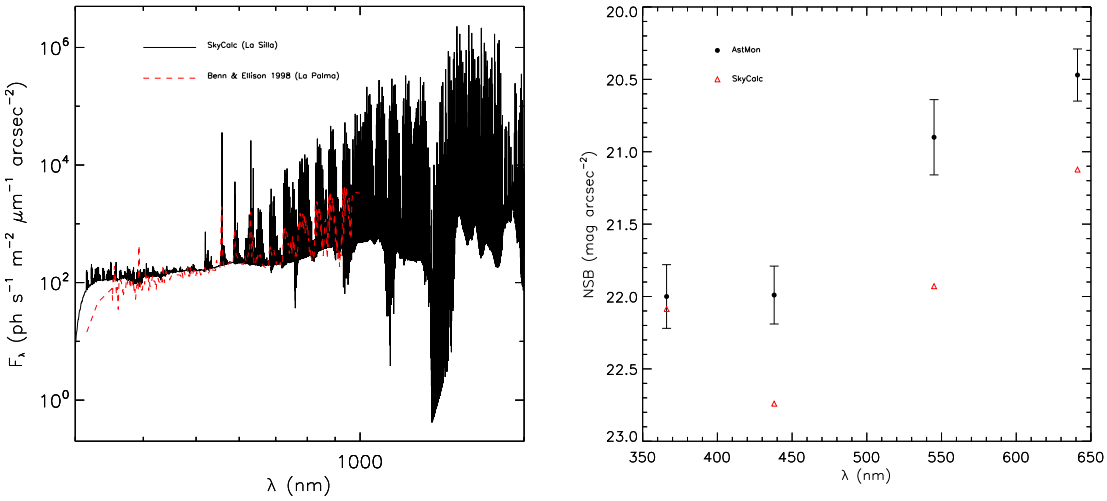

Figure 1: *Left panel:* comparison between the dark NSB synthetic spectrum obtained with SkyCalc (*black solid line*) and the dark NSB spectrum measured by [13] (*red dashed line*). *Right panel:* comparison between the synthetic *UBVR* magnitudes computed from the dark NSB synthetic spectrum at ZA = 0 (*red triangles*) and the equivalent AstMon measurements (*black dots*; see Tab. 1).

To do so, we rely on the NSB measurements taken in the *UBVR* bands with the AstMon telescope[2]. Such measurements cover all the azimuth (Az) directions and a range of ZAs up to ∼45°, and allow the correction of the NSB level in the wavelength range 346 nm ÷ 611 nm. Combining the available measurements in an appropriate way to match the four main cardinal directions in Az (North, East, South, West) and three relevant ZAs (zenith pointing, 20°, and 40°), we produce the set of *UBVR* magnitudes reported in Tab. 1. In Fig. 1, we also show the comparison between such magnitudes towards the zenith and those computed by integrating the dark NSB synthetic spectrum over the *UBVR* passbands. The set of magnitudes for each pointing direction is then normalized to the corresponding magnitudes obtained by convolving the synthetic "dark" NSB spectrum with the relevant passband [14]:

$$\frac{\Phi_{\text{Teide}}}{\Phi_{\text{SkyCalc}}} = 10^{-0.4\left(m_{\text{Teide}} - m_{\text{SkyCalc}}\right)} \tag{1}$$

Interpolating such ratios yields the multiplicative function to the "dark" NSB spectrum that we use to correct for the higher brightness level of the Teide site, getting the (approximated) differential sky brightness in dark conditions.

Finally, we compute the expected NSB photo-electron rates r_{NSB} per pixel for the ASTRI Mini-Array Cherenkov cameras under several Moon conditions. To do so, we add the moonlight synthetic spectra produced by SkyCalc to the "dark" synthetic spectrum rescaled according to Eq. 1 (see Fig. 2), and convolve them with the telescope throughput:

$$r_{\text{NSB}} = \frac{A_{\text{coll}} S_{\text{px}}}{f^2} \cdot \int_{\lambda_1}^{\lambda_2} \text{NSB}_{\text{Teide}}(\lambda) R_1(\lambda) R_2(\lambda) T_{\text{cam}}(\lambda) \text{PDE}(\lambda) d\lambda \tag{2}$$

[2]See http://research.iac.es/OOCC/iac-managed-telescopes/astmon/ for further details.

Band	Zenith	20° N	20° E	20° S	20° W	40° N	40° E	40° S	40° W
U	22.00	22.02	21.91	21.93	21.97	21.99	21.89	21.91	21.96
B	21.99	21.91	21.87	21.88	21.92	21.83	21.76	21.80	21.85
V	20.90	20.79	20.75	20.78	20.82	20.68	20.63	20.67	20.74
R	20.47	20.37	20.33	20.35	20.39	20.25	20.21	20.24	20.30

Table 1: NSB *UBVR* magnitudes for the Teide site.

where $A_{\rm coll} \approx 75,000$ cm^2, $S_{\rm px} = 0.483$ cm^2 and $f = 215.4$ cm are the photon collection area, the pixel geometric area and the telescope phocal length respectively, R_1 and R_2 are the primary- and secondary-mirror reflectivity respectively, $T_{\rm cam}$ is the camera window transparency and PDE is the SiPM photon detection efficiency [15]. We compute Eq. 2 from $\lambda_1 = 200$ nm to $\lambda_2 = 2000$ nm, to take into account the entire SiPM working range; the resulting NSB rates are reported in Tab. 2.

3. Simulations

From the NSB rates derived in Sec. 2, we produce a set of air shower simulations as seen by the ASTRI Mini-Array, focusing on telescope pointing at ZA = 20° and Az = 0° (North). The aim is to get a first evaluation of the impact of such different levels of the NSB on the performance of the system. We consider three main cases (see Tab. 2): (i) dark conditions (indicated as "DARK" in the following); (ii) moderate NSB ("MODERATE"), corresponding to a 60° pointing distance from a half Moon; (iii) high NSB ("HIGH"), corresponding to a 40° pointing distance from an almost full Moon. As a reference, we consider the ASTRI Mini-Array performance curves presented in [16] ("REFERENCE"), in which a preliminary, rather optimistic estimate of the NSB level corresponding to dark conditions at the Teide site was considered.

First, we obtain the average discriminator thresholds (DTs) for the ASTRI Mini-Array cameras by computing the intersection between pure NSB trigger curves corresponding to twice the computed levels and the null-NSB proton trigger curve increased by a factor of 1.5 in normalization; this procedure allows us to derive safe thresholds that prevent camera trigger issues. The obtained values are reported in Tab. 2; in Fig. 2, we also show the comparison between the trigger curves used for this study.

Then, taking advantage of the CoRSiKa [17] and `sim_telarray` simulation software chain [18], we produce MC samples of air showers induced by γ-ray photons (both point-like and diffuse) and electrons with energies from 0.1 up to 330 TeV, and protons with energies from 0.1 up to 600 TeV. Then, we simulate the response of the ASTRI Mini-Array telescopes to these air showers, under the three selected NSB conditions (DARK, MODERATE and HIGH), to get the final MC data samples, basic inputs for the subsequent data reduction and analysis pipeline.

4. Data reduction and analysis

The MC data samples with different levels of the NSB described in Sec. 3 are reduced and analyzed with `A-SciSoft` (version 0.5.8), the scientific software package of the ASTRI Project [19]. After the calibration, at the single-telescope reconstruction step, we identify for each data

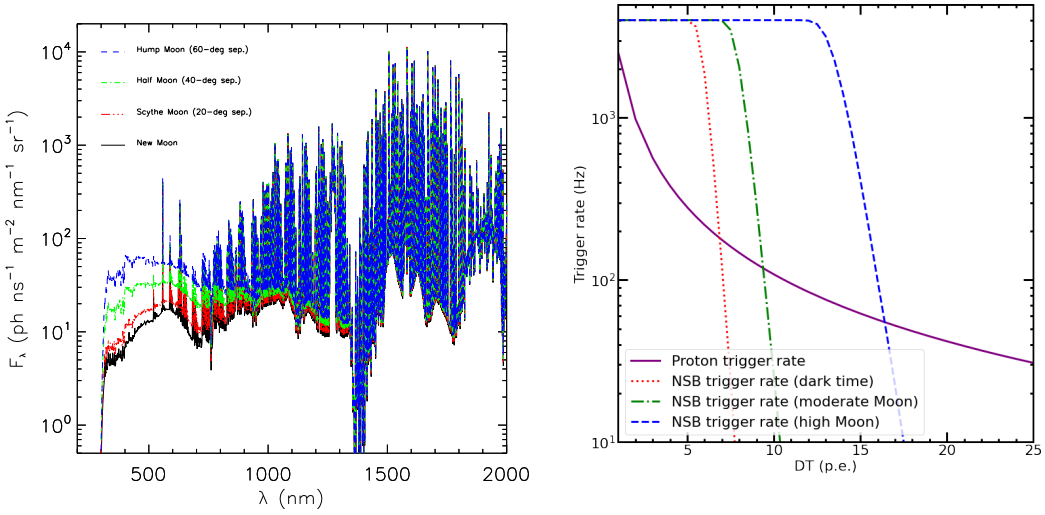

Figure 2: *Left panel:* examples of final NSB synthetic spectra for the Teide site (see text). *Right panel*: discriminator thresholds for different NSB conditions (see Tab. 2).

sample separately suitable image cleaning levels through a scan over a dedicated pedestal run. The final cleaning levels are selected by requiring that no images produced by NSB fluctuations only (computed over 10^4 realizations of pure NSB images) survive the cleaning procedure[3]. The resulting thresholds for the cleaning implemented in the ASTRI pipeline [4] are 10/5 p.e., 13/6.5 p.e., and 23/11.5 p.e., respectively for the DARK, MODERATE, and HIGH data samples.

After the single-telescope data reduction, at the stereoscopic reconstruction level, the background rejection and energy reconstruction are achieved with a procedure based on the random forest (RF) method [20], while the arrival direction of each shower is estimated from the intersection of the major axes of the images from different telescopes.

Once all data samples are fully-reconstructed, we derive the typical performance features of the system in order to assess the impact of increasing levels of the NSB on a comparison basis. To do that, we use the standard software tools and procedure currently implemented in the ASTRI pipeline (see [16] for more details). For all of the considered data samples, we compute the on-axis point-like source differential sensitivity, angular resolution, and energy resolution of the ASTRI Mini-Array for 50 h of observing time in the reconstructed energy range between $10^{-0.5} \simeq 0.3$ TeV and $10^{2.5} \simeq 300$ TeV. We show the results in Fig. 3; a visual inspection reveals performance features (for low ZA observations) that can be summarized as follows:

- the DARK performance is fully comparable with the REFERENCE one, which was obtained with a rather optimistic level of dark NSB [16];

[3]The cleaning method applied to the data is a two-threshold two-pass cleaning. The algorithm first uses a relatively high signal threshold (L1) to search for at least two neighboring pixels – the so-called core pixels – which likely belong to the core of the shower. In a second step, pixels adjacent to core pixels – the so-called boundary pixels – are included in the cleaned image if their signal is above a lower threshold (L2).

Pointing direction	r_{NSB} (ns^{-1})				
	Dark time	Weak Moon	Moderate Moon	Decent Moon	High Moon
Zenith	0.104	0.123	0.204	0.338	0.636
20° North	0.112	0.131	0.211	0.346	0.643
20° East	0.115	0.135	0.215	0.349	0.647
20° South	0.113	0.133	0.213	0.347	0.645
20° West	0.110	0.129	0.210	0.344	0.642
40° North	0.120	0.140	0.220	0.354	0.652
40° East	0.126	0.145	0.226	0.360	0.658
40° South	0.122	0.142	0.222	0.356	0.654
40° West	0.117	0.136	0.216	0.351	0.648
	DT (p.e.)				
20° (average)	6.99	7.60	9.46	12.0	16.4

Table 2: Integrated NSB rates up to 2000 nm for different Moon brightness levels and pointing directions, along with the corresponding DTs for the ASTRI Mini-Array camera.

- the MODERATE performance lies within a factor of ∼2 with respect to the DARK one in the range 1 TeV ÷ 10 TeV, and becomes comparable above 10 TeV;
- above 10 TeV, all NSB conditions do not relevantly impact on angular and energy resolutions;
- The ASTRI Mini-Array will be able to perform observations under high NSB conditions with a sensitivity within a factor of ∼2 (and comparable angular/energy resolution) with respect to the one achievable in dark NSB conditions above ∼10 TeV.

Such findings, together with what is found for the MODERATE performance, permit to consider a relevant enhancement of the system duty cycle, in particular for deep observations of galactic targets aimed at constraining the emission models at multi-TeV energies [21].

5. Summary and outlook

In this contribution, we have presented the first study for the determination of the ASTRI Mini-Array performance at the *Observatorio del Teide* site under different NSB conditions, established via the production of synthetic NSB spectra that have been rescaled to actual brightness measurements of the Teide night sky. Through the use of the standard ASTRI Mini-Array simulation and analysis chains, we first produced images of Cherenkov showers that are affected by increasing NSB levels, and then derived the expected performance for each illumination condition. The outcomes of this study suggest that the ASTRI Mini-Array will be able to observe targets under high NSB conditions (up to ∼6 times the dark NSB ones) with acceptable performance losses (at ZA = 20°) with respect to the dark nights above ∼10 TeV, thus significantly extending the useful observing time window of the facility without the need of specific hardware requirements.

The analysis presented here is somewhat conservative, since image cleaning and stereo reconstruction methods can be better optimized for MODERATE and, especially, HIGH samples. On the

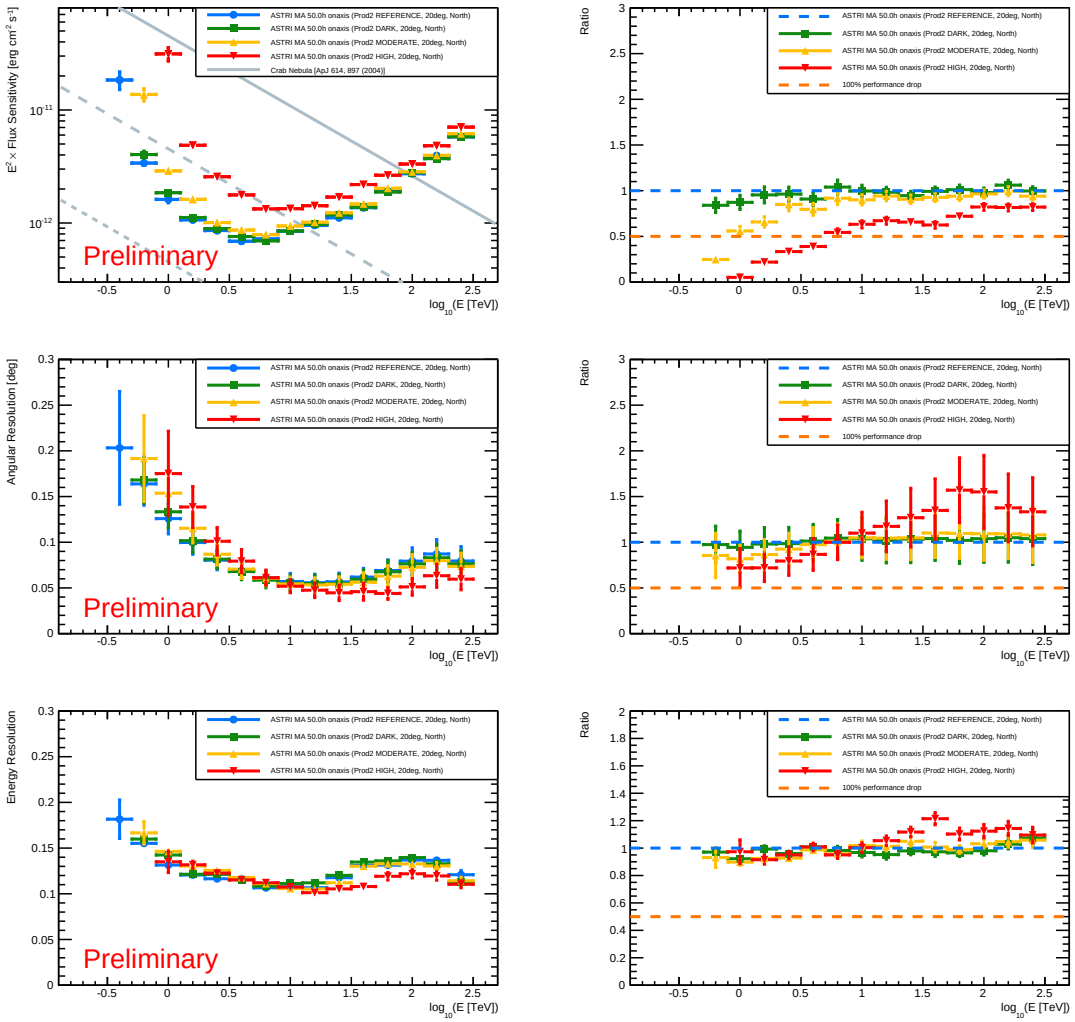

Figure 3: *Upper panels:* ASTRI Mini-Array on-axis point-like source differential sensitivity (*left*), at ZA = 20° and Az = 0°, for four different analyses: REFERENCE (*blue circles*), DARK (*green squares*), MODERATE (*yellow upward triangles*), HIGH (*red downward triangles*), along with the ratios between the sensitivity obtained by DARK, MODERATE, and HIGH analysis and that of REFERENCE (*right*). The Crab Nebula spectral model (*grey lines*) is taken from [22]. *Middle panels:* ASTRI Mini-Array on-axis point-like source angular resolution (*left*) for the same analyses, along with the corresponding ratios (*right*). *Lower panels:* ASTRI Mini-Array on-axis point-like source energy resolution (*left*) for the four different analyses, along with the corresponding ratios (*right*). In all panels, the ratios are calculated so that higher values correspond to better performance. In the right panels, the ratio levels corresponding to no performance drops (*blue dashed lines*) and 100% performance drops (*orange dashed lines*) are indicated.

other hand, no off-axis performance studies are at present available. Such topics will be investigated in the prosecution of this work, where also pointings at higher ZAs will be simulated and analyzed. Finally, since with the presently available data we are unable to quantify possible discrepancies between the synthetic "dark" NSB spectrum and the actual Teide sky brightness for wavelengths greater than ~700 nm and ZA > 45°, an extension of the AstMon measurements at the Teide site has to be planned in the near future to provide crucial NSB measurements at larger wavelengths ($IJHKL$ bands) and higher ZAs.

Acknowledgments

This work was conducted in the context of the ASTRI Project. We gratefully acknowledge support from the people, agencies, and organisations listed here: http://www.astri.inaf.it/en/library/. We acknowledge financial support from the ASI-INAF agreement no. 2022-14-HH.0. This paper went through the internal ASTRI review process.

References

[1] S. Scuderi *et al.*, JHEAp **35**, 52 (2022).

[2] A. Giuliani *et al.*, Proc. 38th ICRC (Nagoya, Japan), PoS(ICRC2023)892 (2023).

[3] M. de Naurois & D. Mazin, C. R. Phys. **16**, 610 (2015).

[4] S. Lombardi *et al.*, A&A **634**, A22 (2020).

[5] G. Leto *et al.*, Proc. 38th ICRC (Nagoya, Japan), PoS(ICRC2023)729 (2023).

[6] F. G. Saturni *et al.*, Proc. 38th ICRC (Nagoya, Japan), PoS(ICRC2023)719 (2023).

[7] MAGIC Coll., Astropart. Phys. **94**, 29 (2017).

[8] M. Aubé *et al.*, MNRAS **497**, 2501 (2020).

[9] S. Noll *et al.*, A&A **543**, A92 (2012).

[10] A. Jones *et al.*, A&A **560**, A91 (2013).

[11] P. Yoachim *et al.*, Proc. SPIE **9910**, 99101A (2016).

[12] K. Leschinski & J. Alves, A&A **639**, A120 (2020).

[13] C. R. Benn & S. L. Ellison, New Astron. Rev. **42**, 503 (1998).

[14] M. S. Bessell *et al.*, A&A **333**, 231 (1998).

[15] G. Romeo *et al.*, Nucl. Inst. and Meth. in Phys. Res. A **908**, 117 (2018).

[16] S. Lombardi *et al.*, PoS **395**, 884 (2022).

[17] D. Heck *et al.*, *CORSIKA: a Monte Carlo code to simulate extensive air showers*, TIB Hannover (1998).

[18] K. Bernlöhr, Astropart. Phys. **30**, 149 (2008).

[19] S. Lombardi *et al.*, Proc. SPIE **10707**, 107070R (2018).

[20] L. Breiman, Mach. Learn. **45**, 5 (2001).

[21] S. Vercellone *et al.*, JHEAp **35**, 1 (2022).

[22] F. Aharonian *et al.*, ApJ **614**, 2 (2004).